Eur. Phys. J. E **5**, 337–351 (2001)

THE EUROPEAN PHYSICAL JOURNAL E

EDP Sciences

Scaling theory of mixed amphiphilic monolayers

Shigeyuki Komura[1,2,a] and S.A. Safran[2,b]

[1] Department of Chemistry, Faculty of Science, Tokyo Metropolitan University, Tokyo 192-0397, Japan
[2] Department of Materials and Interfaces, Weizmann Institute of Science, Rehovot 76100, Israel

Received 29 December 2000 and Received in final form 19 March 2001

Abstract. We predict the elastic properties of mixed amphiphilic monolayers in the swollen state within the blob model using scaling arguments. First the elastic moduli and the spontaneous curvature of a bimodal brush are determined as a function of the composition and the relative chain length. We obtain simple and useful scaling functions which interpolate between the elastic moduli of a pure short-chain brush and a pure long-chain brush. By using the analogy between block copolymer interfaces and polymeric brushes, the effect of mixing on self-assembled diblock copolymer monolayers is investigated in the swollen state. We calculate various interfacial properties, such as the equilibrium surface coverage, interface curvature, and the mixing free energy as a function of the composition. In general, we find a nonlinear dependence on the composition, which deviates from the simple linear averaging of the properties of pure components. Our results are used to discuss a recent experiment on the effect of amphiphilic block copolymers on the efficiency of microemulsions.

PACS. 36.20.-r Macromolecules and polymer molecules – 68.05.-n Liquid-liquid interfaces – 82.70.-y Disperse systems; complex fluids

1 Introduction

There are many technological applications of self-assembled amphiphiles such as their use as stabilizers of two immiscible solvents, or equilibrium vesicles for encapsulation. Accurate control of the interfacial properties is thus necessary to utilize these materials. The most basic and important physical property of an adsorbed amphiphilic layer at a liquid-liquid interface is its preferred interfacial curvature. A formal expansion of the free energy *per unit area* of a bent surface up to quadratic order in the curvatures is written as [1,2]

$$F_{\rm b}(c_1,c_2)=\frac{\kappa}{2}(c_1+c_2-2c_0)^2+\kappa_{\rm G}c_1c_2. \tag{1.1}$$

Here c_1 and c_2 are two principle curvatures, κ and $\kappa_{\rm G}$ are the bending and Gaussian moduli, respectively, and c_0 is the spontaneous curvature. The quantities $(c_1+c_2)/2$ and c_1c_2 are the mean curvature and Gaussian curvature, respectively. The free energy expresses the fact that the mean curvature that minimizes $F_{\rm b}$ has a value c_0 when $\kappa_{\rm G}=0$. Much progress has been made in understanding the thermodynamics, structural, and dynamic properties of microemulsions and surfactant membranes using the concept of curvature energy [3–5].

[a] e-mail: komura@comp.metro-u.ac.jp
[b] e-mail: sam.safran@weizmann.ac.il

In addition to short-chain surfactants, long-chain polymers can sometimes also show surfactant-like behavior [6]. Examples include block copolymers, where two or more incompatible polymers are chemically joined together [7]. When mixed with two incompatible homopolymers or small-molecule solvents which are also selective for the two blocks, these copolymers can function as compatibilizers and thus make stable microemulsions [8–11]. Due to their temperature stability and high efficiency in reducing the interfacial tension, it is sometimes preferable to use these long-chain polymeric surfactants.

1.1 Monodisperse interfaces

The curvature elasticity of monodisperse diblock copolymer monolayers or bilayers has been widely investigated theoretically. There are several approaches to this problem. One of them is to utilize the analogy between block copolymer interfaces and polymeric brushes, namely, chains that are irreversibly anchored by one end to an impenetrable surface [12–14]. (A short review of theoretical works on brushes will be provided in the next section.) Once the stretching energy of a brush is known, the stretching energy for a copolymer layer can be simply obtained by adding the stretching energy of the two diblock sections. Wang and Safran [15] calculated the elastic moduli of the diblock copolymer monolayers under *melt*

(no solvent) condition by using the results from the self-consistent field theory (SCFT) of a brush [16–20]. They also studied the onset and morphology of various equilibrium emulsion phases for an A and B homopolymer mixture with AB diblock copolymers [15].

Similar calculations have been done for *swollen* monolayers of diblock copolymers which can be obtained if the two solvents are good for one of the blocks and poor for the other, and if the molecular weight of the solvents are small compared to the blocks. This case was first considered by Cantor [21]. Leibler later treated the problem of a random dispersion of A and B homopolymers by a small amount of AB block copolymer [22,23]. In a different paper by Wang and Safran [24], within the SCFT employing a scaling-augmented free-energy functional [16, 17], the elastic moduli and the spontaneous curvature for monolayers of diblock copolymers under swollen condition was calculated.

In the case of self-assembled monolayers, the surface density adjusts itself to minimize the total free energy which includes both the chain stretching contribution and the interfacial energy [15,24]. This is different from grafted polymer brushes whose surface density is fixed *a priori*. References [15,24] showed that, for both the melt and swollen states, the surface density decreases with the molecular weight of the chain, whereas the interface curvature increases with the molecular weight ratio of the two blocks. Hence the control of the overall molecular weight or asymmetry leads to the manipulation of the interfacial properties. However, synthesis of many different types of copolymer chains, each with different molecular weights or symmetries, is a formidable task and may be impractical.

1.2 Mixed interfaces

Another way to control the interfacial properties is to mix different types of amphiphilic molecules through composition variation. For low molecular surfactants, it was shown that a mixture of surfactants can spontaneously form large bilayer vesicles, whereas the single components do not [25]. The appearance of equilibrium vesicles in mixtures of surfactants is explained by a phenomenological model [26–28] where the spontaneous curvature c_0 is dependent on the monolayer composition (so-called "curvature instability"). This idea was further extended by Dan and Safran [29,30] to the amphiphilic interfaces consisting of mixture of diblock copolymers in the *melt* state.

Recently, a very interesting experiment by Jakobs *et al.* has shown that amphiphilic block copolymers (PEP-PEO) dramatically enhance the solubilization capacity of medium-chain surfactants (C_iE_j) in ternary (oil/water/surfactant) microemulsions [31]. By adding small fractions of amphiphilic block copolymers, the minimum amount of surfactant (C_iE_j) needed to form a one-phase microemulsion is greatly reduced. More recent small-angle neutron scattering experiments demonstrated that the copolymers sometimes form mushroom conformations (where the polymer chains do not overlap each other) on both sides of the surfactant monolayer [32]. In that paper, the observed solubility enhancement is attributed to the variation of the elastic moduli κ and κ_G, which has been calculated by Lipowsky and coworkers for mushroom conformations of anchored (end-grafted) polymers [33,34].

The assumption of a uniform curvature distribution is correct only when the mushrooms just begin to overlap. At relatively higher copolymer concentrations in the experiment, however, the copolymers start to form brushes and the mushroom picture breaks down [32]. In this case, the monolayers in the microemulsions can be regarded as brushes comprising a mixture of short (surfactant) and long (polymer) amphiphilic diblock copolymers in the swollen state. The curvature elasticity of mixed brushes in the swollen case has not yet been studied, although there is a calculation for the melt case [19]. It is therefore desirable to consider the theory of the elastic moduli of mixed diblock copolymer monolayers in the swollen state.

1.3 The present work

In this paper, we discuss the elastic properties of mixed amphiphilic monolayers within the blob picture. By using scaling arguments, we first extend the results in references [33,34] to a bimodal brush (a mixture of shorter and longer chains) in order to calculate its elastic moduli and spontaneous curvature in the *swollen* state. In contrast to the fairly complicated results for the elastic moduli of a bimodal brush in the *melt* state [19], we obtain a simple and useful scaling functions which interpolate between those of a pure short-chain brush and a pure long-chain brush [35]. We then make use of the analogy between block copolymer interfaces and polymeric brushes and add the stretching energy of the two diblock sections to calculate the stretching energy of mixed amphiphilic monolayers composed of two types of diblock copolymers. Using arguments similar to those of reference [30] (that treats the *melt* case), we discuss the effect of mixing on self-assembled diblock copolymer monolayers in the *swollen* state. By taking into account the fact that the surface density adjusts itself to minimize the total free energy, we calculate the equilibrium surface coverage, interface curvature, and the free energy as a function of the composition. In general, we find a nonlinear dependence of these quantities on the composition, which deviates from the simple linear averaging of the pure component monolayers.

Our work can be regarded in part as an extension of the work by Dan and Tirrell who considered the phase behavior of *monodisperse* diblock copolymer microemulsions [36]. Within a scaling model, they showed that symmetric copolymers form lamellar interfaces, whereas asymmetric copolymers aggregate in spherical microdomains. In the present work, we concentrate on the effect of mixing on bimodal diblock copolymer microemulsions.

This paper is organized as follows. We first give a brief review of the theoretical work on end-grafted brushes. In section 3, we discuss the elastic properties of a bimodal brush in the swollen state within the scaling theory. We calculate the free energy of the bimodal brush for the flat,

spherical, and cylindrical cases. Using this result, we extract the elastic moduli and the spontaneous curvature from a curvature expansion. The effect of mixing on self-assembled amphiphilic monolayers is considered in section 4. Various surface properties are calculated there by the minimization of the chain stretching energy. The paper ends with a summary and a discussion of the experiments by Jakobs *et al.* [31,32] in light of our result.

2 Previous work on monodisperse brushes

Before explaining our calculations, we briefly summarize some previous theoretical work on monodisperse polymeric brushes [6]. This is useful since the analogy between polymeric brushes and block copolymer interfaces is utilized later in this paper. A brush on a flat surface was first considered by de Gennes [12,13] within a mean-field theory. When all the chains are of the same molecular weight N (monodisperse brush), he showed that, as a function of molecular weight N and surface coverage Γ (see Eq. (3.2) below), the height of the brush scales as $N\Gamma^{1/3}$ and the free energy *per unit area* scales as $N\Gamma^{5/3}$. Subsequently, Alexander introduced the blob picture for a polymer brush and developed a scaling theory [14]. He predicted the same scaling for the height $N\Gamma^{1/3}$, whereas the free energy *per unit area* is shown to scale as $N\Gamma^{11/6}$. The difference in the free energy reflects the fact that the mean-field theory overestimates both repulsive and attractive terms in the same manner.

An important development in this field was advanced by Milner and his coworkers [16,17] by applying self-consistent field theory (SCFT) to polymeric brushes based on the work of Semenov [37]. The SCFT exploits the fact that in the limit of strong stretching, the partition function of the brush is dominated by the "classical paths" of the chains, and random-walk fluctuations about these paths can be neglected. Their work goes beyond the Alexander-de Gennes theory in several aspects; for example, it was shown that the density profile is parabolic [16,17] rather than a step-function [12–14]. However, for chains at moderate concentration in a not-too-good solvent (referred to as the "moderate density case"), the scaling behavior of the brush height and the free energy is the same with the mean-field theory by de Gennes mentioned above. (Hence this case is sometimes called as the mean-field version of SCFT.) The SCFT of swollen brushes has been also considered by using a scaling-augmented free-energy functional [16,17].

More recently, Lipowsky and his coworker investigated the effects of the addition of anchored polymers on bilayer membranes and calculated the changes in the bending moduli and the spontaneous curvature due to the polymers [33,34]. By considering anchored polymers in the mushroom regime (low polymer coverage) and the brush regime (high polymer coverage) separately, they found that, in both cases, the bending modulus κ increases, whereas the Gaussian modulus $\kappa_{\rm G}$ decreases. Similar theoretical results have been also reported in other works [38,39]. Note that these results are in contrast to the previous theoretical works on the effect of *adsorbed* polymers on membranes [40–43], where the bending modulus decreases and the Gaussian modulus increases due to the polymers. The effect of adding polymers to both sides of the membrane have been considered in references [44,45]. The increase in the bending modulus of the polymer decorated membranes has been confirmed by several experiments [46–52].

3 Mixed swollen brushes: a scaling theory

In this section, we consider a bimodal brush in the *swollen* state using a scaling argument in which each chain is treated as a string of blobs [53]. Brushes are formed when the mean distance between the polymer chains is smaller than the radius of the polymer coil so that they overlap each other. Our goal in this section is to calculate the elastic moduli and the spontaneous curvature of a swollen bimodal brush by extending the scaling arguments in references [33,34] to a bimodal brush. We obtain simple scaling functions which interpolate between the bending moduli of a pure short-chain brush and a pure long-chain brush. Our results will be compared with those derived using the SCFT for mixed brushes [18,19].

We consider a bimodal brush containing a fraction ϕ of longer chains of molecular weight $N_{\rm L}$ and a fraction $(1-\phi)$ of shorter chains of molecular weight $N_{\rm S}$ ($N_{\rm S} < N_{\rm L}$). If the total number of polymer chain (including both longer and shorter chains) is denoted by X, there are $X\phi$ longer chains and $X(1-\phi)$ shorter chains. Both chains are assumed to have the same segment length a. We define a measure of the molecular weight difference between the two chains as

$$\alpha \equiv \frac{N_{\rm L} - N_{\rm S}}{N_{\rm S}}. \tag{3.1}$$

Hence $N_{\rm L}$ and $N_{\rm S}$ are related by $N_{\rm L} = (1+\alpha)N_{\rm S}$. The size of a polymer chain is characterized by the mean end-to-end distance $R \approx aN^{\nu}$ of the polymer in solution, where ν is the correlation exponent. In this paper, we are mainly interested in polymer brushes under good solvent conditions and consider the swollen brush case. Hence, within the Flory approximation, the corresponding exponent ν has the numerical value $\nu \simeq 3/5$.

The distance between the grafting points is denoted ξ_0. Then it is convenient to introduce the reduced surface coverage Γ given by

$$\Gamma \equiv \left(\frac{a}{\xi_0}\right)^2, \tag{3.2}$$

which gives the dimensionless number of polymer chains per unit area. The reduced overlap coverage scales as $\Gamma_{\rm ov} \sim N_{\rm S}^{-2\nu}$. The mushroom regime, applicable to non-overlapping chains, extends from $\Gamma = 0$ up to $\Gamma = \Gamma_{\rm ov}$ [33,34]. For $\Gamma > \Gamma_{\rm ov}$, the chains overlap to form a brush and the polymers experience an additional loss of entropy arising from the steric confinement by the neighboring chains.

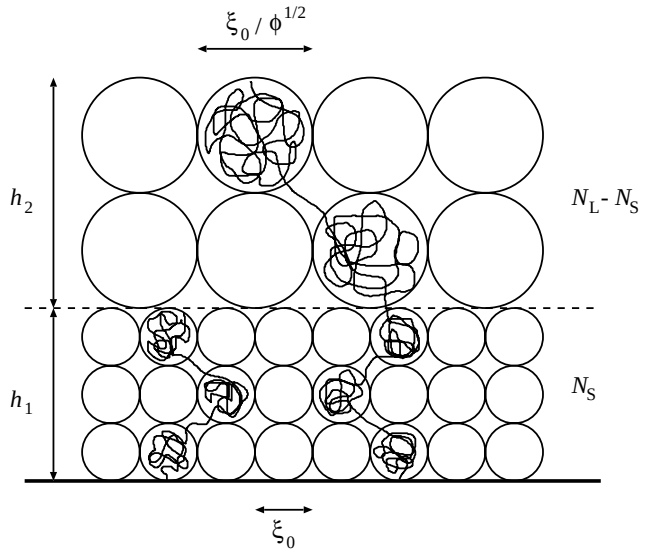

Fig. 1. Scaling picture of a bimodal polymer brush on a flat surface. The height of the first layer (closer to the grafting surface) is h_1 and that of the second layer is h_2. In the second layer, $(N_L - N_S)$ monomers are "dawdling" beyond h_1. The distance between the anchor points is ξ_0 on the grafting surface. In the second layer, the blob size increases discontinuously to $\xi_0/\phi^{1/2}$ where ϕ is the fraction of longer chains.

The free ends of the chains must be segregated vertically by molecular weight and the brush consists of two layers of blobs as shown in Figure 1. This is the case considered in this section.

However, it is important to note that we cannot use the brush model in the limit of only a few long chains. In our theory, we will assume that the long chains on top of the short ones form a brush, which is only true if the long chains are close enough to overlap. For the second upper layer one may define an effective coverage $\Gamma' = \Gamma\phi$ where Γ is given by (3.2). Hence Γ' vanishes for $\phi \to 0$. The overlap coverage for the second layer scales as $\Gamma'_{ov} \sim (N_L - N_S)^{-2\nu}$. If the long chains are too dilute, they are effectively isolated and do not form a brush. For this case, the mushroom (on top of a brush) picture is relevant and will be discussed in section 5 separately.

3.1 Flat surface

Consider a bimodal brush on a flat surface for which the free ends of the shorter chains are found at distances closer to the grafting surface than those of the longer chains as in Figure 1 [18,19]. The first layer, which is closer to the grafting surface, consists of blobs containing both shorter and longer chains, whereas the second layer consists of blobs containing only longer chains. In the first layer, each blob is of radius ξ_0 and contains $(\xi_0/a)^{1/\nu}$ segments. The number of blobs is equal to h_1/ξ_0 where h_1 is the height of the first layer (see Fig. 1) and satisfies

$$N_S = h_1 \left(\frac{\xi_0}{a}\right)^{1/\nu} \frac{1}{\xi_0}. \tag{3.3}$$

By solving this equation for h_1 and using (3.2), we obtain

$$h_1 = N_S a^{1/\nu} \xi_0^{1-1/\nu} = a N_S \Gamma^{(1-\nu)/2\nu}. \tag{3.4}$$

This expression for the height is the same as equation (46) in reference [34] and scales as $N_S\Gamma^{1/3}$ for $\nu = 3/5$, which is in agreement with results for monodisperse brushes mentioned in section 3.

In the second, upper layer, $(N_L - N_S)$ monomers are "dawdling" beyond h_1. These extra $(N_L - N_S)$ monomers are analogous to a chain of $(N_L - N_S)$ segments attached to a wall at h_1. However, the effective grafting distance is larger than that of the first layer, and is given by the distance between long chains, $\xi_0/\phi^{1/2}$, due to the two-dimensional nature of the surface. Similar to (3.3), the height of the second layer h_2 (see Fig. 1) satisfies the following relation:

$$N_L - N_S = h_2 \left(\frac{\xi_0/\phi^{1/2}}{a}\right)^{1/\nu} \frac{1}{\xi_0/\phi^{1/2}}. \tag{3.5}$$

Hence we obtain

$$h_2 = (N_L - N_S) a^{1/\nu} \xi_0^{1-1/\nu} \phi^{(1-\nu)/2\nu} = a(N_L - N_S)\Gamma^{(1-\nu)/2\nu}\phi^{(1-\nu)/2\nu}. \tag{3.6}$$

From (3.4) and (3.6), h_1 and h_2 are related by

$$h_2 = \alpha \phi^{(1-\nu)/2\nu} h_1, \tag{3.7}$$

which will be used later to eliminate h_2.

Next, we consider the free energy which is proportional to the number of blobs. Let us denote the total area of the grafting surface by A. There are A/ξ_0^2 and $A/(\xi_0^2/\phi)$ chains in the first and the second layer, respectively. Notice that A/ξ_0^2 is equal to the total number of chains X. Since the number of blobs is proportional to h_1/ξ_0 and $h_2/(\xi_0/\phi^{1/2})$ in the first and the second layer, respectively, the *total* free energy of the system (aside from a numerical factor of order unity) is given by

$$\tilde{F}_0 = T\left[\left(\frac{A}{\xi_0^2}\right)\left(\frac{h_1}{\xi_0}\right) + \left(\frac{A}{\xi_0^2/\phi}\right)\left(\frac{h_2}{\xi_0/\phi^{1/2}}\right)\right] = T\left(\frac{A}{\xi_0^2}\right)\left(\frac{h_1}{\xi_0}\right)\left[1 + \alpha\phi^{(1+2\nu)/2\nu}\right], \tag{3.8}$$

where we have used (3.7) to eliminate h_2, and T is the temperature measured in energy units. (The Boltzmann constant k_B is contained in T.) The above energy accounts for chain stretching and excluded-volume interactions of the bimodal brush. By using (3.2) and (3.4), the free energy *per unit area* $F_0 = \tilde{F}_0/A$ is then given by

$$F_0 = \frac{T h_1}{\xi_0^3} f_0(\alpha,\phi) = \frac{T}{a^2} N_S \Gamma^{(1+2\nu)/2\nu} f_0(\alpha,\phi), \tag{3.9}$$

where we define the function $f_0(\alpha,\phi)$ by

$$f_0(\alpha,\phi) = 1 + \alpha\phi^{(1+2\nu)/2\nu}. \tag{3.10}$$

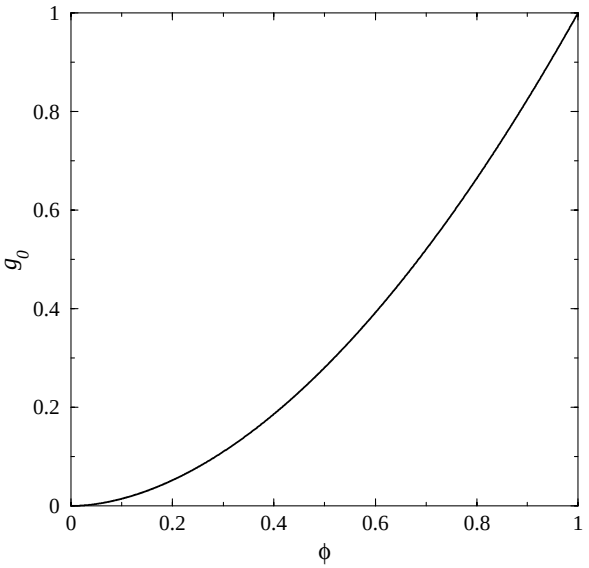

Fig. 2. Plot of $g_0 \equiv [f_0(\alpha,\phi)-1]/[f_0(\alpha,\phi=1)-1] = \phi^{11/6}$ as a function of ϕ (fraction of longer chains). The function $f_0(\alpha,\phi)$ is defined in (3.12).

For $\nu = 3/5$, (3.9) and (3.10) becomes

$$F_0 = \frac{T}{a^2} N_{\rm S} \Gamma^{11/6} f_0(\alpha,\phi), \tag{3.11}$$

and

$$f_0(\alpha,\phi) = 1 + \alpha\phi^{11/6}, \tag{3.12}$$

respectively. Notice that $f_0 = 1$ for either $\alpha = 0$ (monodisperse brush) or $\phi = 0$ (pure short-chain brush). In this limit the above scaling behavior coincides with that given by Alexander [14] or by equation (47) in reference [34] (note also [54]). It is easy to see that for $\phi = 1$ (pure long-chain brush), we have $F_0 = (T/a^2)N_{\rm L}\Gamma^{(1+2\nu)/2\nu}$ as it should be.

The behavior of the function $g_0 \equiv [f_0(\alpha,\phi)-1]/[f_0(\alpha,\phi=1)-1] = \phi^{11/6}$ is shown in Figure 2. Notice that g_0 does not depend on α, and the slope of g_0 vanishes for small ϕ. For ϕ near unity, the curve drops more steeply than a linear interpolation between the pure brushes ($\phi = 0$ and 1). These facts indicate that, as far as the free energy of the flat bimodal brush is concerned, adding a small fraction of shorter chains is much more effective than the addition of a small fraction of longer chains as has been pointed out before [18,19,29,30].

One can compare (3.11) with the free energy of a bimodal brush obtained within the SCFT [18]. For the moderate density case, their result of the free energy per unit area scales as $N_{\rm S}\Gamma^{5/3}[1+\alpha\phi^{5/3}]$. The small differences between our results and those of SCFT are of order $\Gamma^{1/6}$ and $\phi^{1/6}$ and are due to correlation effects that are neglected in the mean-field version of the SCFT used for the case of moderate density [18].

By subtracting the free energy of two separate assemble of brushes made of the pure $N_{\rm L}$ and $N_{\rm S}$ chains, we obtain the free energy of mixing as

$$\Delta F_0 = \frac{T}{a^2}(N_{\rm L}-N_{\rm S})\Gamma^{11/6}\left[\phi^{11/6}-\phi\right]. \tag{3.13}$$

As long as Γ is fixed, this free energy is minimized for $\phi = (6/11)^{6/5} \approx 0.483$.

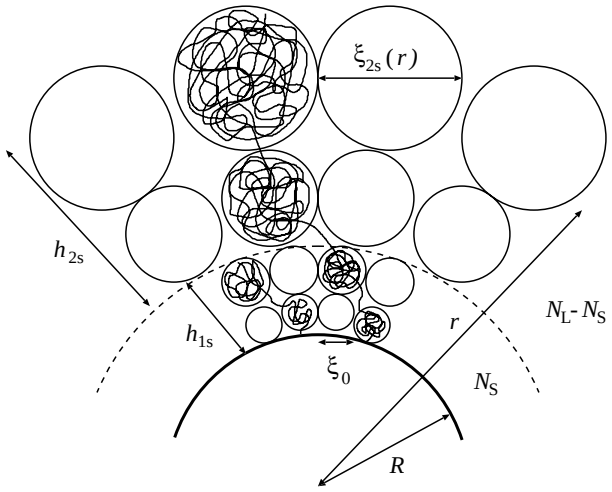

Fig. 3. Scaling picture of a bimodal polymer brush on a spherical surface of radius R. The height of the first layer (closer to the grafting surface) is h_{1s} and that of the second layer is h_{2s}. In the second layer, $(N_{\rm L}-N_{\rm S})$ monomers are "dawdling" beyond h_{1s} as in Figure 1. The distance between the anchor points is ξ_0 on the grafting surface. The blob size scales as $\xi_{1s}(r) = \xi_0 r/R$ in the first layer and $\xi_{2s}(r) = \xi_0 r/(R\phi^{1/2})$ in the second layer, where r is the distance from the center of the sphere (see (3.14)).

3.2 Spherical surface

In order to obtain the elastic moduli and the spontaneous curvature, one has to extend the scaling argument for a bimodal brush grafted on spherical and cylindrical surfaces. A polymer brush on a sphere or a cylinder consists of concentric layers of blobs. As in the flat surface case, a bimodal brush on curved surfaces also consists of two layers. This is illustrated in Figure 3 for a spherical surface. Let us denote the size of blobs in the first and the second layer by $\xi_{1i}(r)$ and $\xi_{2i}(r)$, respectively, where r is the distance from the center of the sphere, and i = s and i = c for spherical and cylindrical geometries, respectively. In each of the layers, the size of the blobs increases with the distance from the grafting surface. In the first layer the surface area is given by $S(r) \approx X\xi_{1i}(r)^2$, where X is the total number of polymer chains, whereas in the second layer it is $S(r) \approx X\phi\xi_{2i}(r)^2$ since the second layer consists of $X\phi$ longer polymer chains. These relations hold both for the spherical and the cylindrical cases.

For a sphere of radius R, $S(r) = 4\pi r^2$ and $X = 4\pi R^2/\xi_0^2$ where ξ_0 is the distance between grafting points. Using these relations, we obtain the blob size as a function

of concentration from

$$\xi_{1s}(r) = \frac{\xi_0 r}{R}, \qquad \xi_{2s}(r) = \frac{\xi_0 r}{R\phi^{1/2}}, \tag{3.14}$$

in each of the layer. Each blob contains $[\xi_{1s}(r)/a]^{1/\nu}$ and $[\xi_{2s}(r)/a]^{1/\nu}$ segments in the first and the second layer, respectively.

As described in appendix A, we follow a similar procedure as in the flat surface and obtain the free energy *per unit area*

$$F_s(R) = \frac{T}{a^2} N_S \Gamma^{(1+2\nu)/2\nu} f_s\left(\frac{h_1}{R}\right), \tag{3.15}$$

with

$$f_s(x) = \frac{\nu}{x}\log\left(1+\frac{x}{\nu}\right) + \phi^{3/2}\frac{\nu}{x}\log\frac{1+(x/\nu)\big(1+\alpha\phi^{(1-\nu)/2\nu}\big)}{1+(x/\nu)}. \tag{3.16}$$

For either $\alpha = 0$ (monodisperse brush) or $\phi = 0$ (pure short-chain brush), the above result reduces to equation (50) in reference [34]. (We did not subtract the free energy of the flat brush (3.9).) Our results generalize this to the case of the *mixed* polymer brush. We note here that the equations such as (A.3), (A.6), (3.15) will not change even if we include additional dimensionless coefficients in N_S (N_L) or F_s [34].

3.3 Cylindrical surface

Here we repeat a similar argument for a bimodal brush on a cylindrical surface of radius R and length D. The surface area of a cylinder is now $S(r) = 2\pi D r$ and $X = 2\pi DR/\xi_0^2$. Hence the blob size varies as

$$\xi_{1c}(r) = \frac{\xi_0 r^{1/2}}{R^{1/2}}, \qquad \xi_{2c}(r) = \frac{\xi_0 r^{1/2}}{R^{1/2}\phi^{1/2}}, \tag{3.17}$$

in each of the layer. Each blob contains $[\xi_{1c}(r)/a]^{1/\nu}$ and $[\xi_{2c}(r)/a]^{1/\nu}$ segments in the first and the second layer, respectively.

As described also in appendix A, we follow a similar procedure as in the spherical surface and obtain the free energy *per unit area*

$$F_c(R) = \frac{T}{a^2} N_S \Gamma^{(1+2\nu)/2\nu} f_c\left(\frac{h_1}{2R}\right), \tag{3.18}$$

with

$$f_c(y) = \frac{1}{y}\left[\left(1+\frac{1+\nu}{\nu}y\right)^{\nu/(1+\nu)} - 1\right] + \phi^{3/2}\frac{1}{y}\left[\left\{1+\frac{1+\nu}{\nu}y\big(1+\alpha\phi^{(1-\nu)/2\nu}\big)\right\}^{\nu/(1+\nu)} - \left(1+\frac{1+\nu}{\nu}y\right)^{\nu/(1+\nu)}\right]. \tag{3.19}$$

For either $\alpha = 0$ (monodisperse brush) or $\phi = 0$ (pure short-chain brush) the above result reduces to equation (53) in reference [34]. Our results generalize this to the case of a *mixed* polymer brush.

We comment here that the same scaling picture can be also applied to a bimodal brush grafted to the inside of a sphere or a cylinder as long as the innermost blob is larger than a. (See the more detailed discussion in reference [34].)

3.4 Small curvature expansion

Here we determine the elastic moduli and the spontaneous curvature of a bimodal brush by expanding the free energies in (3.15) and (3.18) up to second order in h_1/R. For the spherical geometry, we have

$$F_s(R) \approx \frac{T}{a^2} N_S \Gamma^{(1+2\nu)/2\nu} \times\left[f_0(\alpha,\phi) - \frac{1}{2\nu}f_1(\alpha,\phi)x + \frac{1}{3\nu^2}f_2(\alpha,\phi)x^2 + \cdots\right] \tag{3.20}$$

with $x = h_1/R$ and Γ is the surface coverage. For cylindrical geometry, we find

$$F_c(R) \approx \frac{T}{a^2} N_S \Gamma^{(1+2\nu)/2\nu} \times\left[f_0(\alpha,\phi) - \frac{1}{2\nu}f_1(\alpha,\phi)y + \frac{\nu+2}{6\nu^2}f_2(\alpha,\phi)y^2 + \cdots\right] \tag{3.21}$$

with $y = h_1/2R$. In the above, $f_0(\alpha,\phi)$ is given by (3.10), and $f_1(\alpha,\phi)$ and $f_2(\alpha,\phi)$ are defined as

$$f_1(\alpha,\phi) = 1 + 2\alpha\phi^{(1+2\nu)/2\nu} + \alpha^2\phi^{(2+\nu)/2\nu}, \tag{3.22}$$

$$f_2(\alpha,\phi) = 1 + 3\alpha\phi^{(1+2\nu)/2\nu} + 3\alpha^2\phi^{(2+\nu)/2\nu} + \alpha^3\phi^{3/2\nu}. \tag{3.23}$$

Since $f_1 = f_2 = 1$ for either $\alpha = 0$ (monodisperse brush) or $\phi = 0$ (pure short-chain brush), (3.22) and (3.23) coincide in this limit with equations (59) and (60) in reference [34], respectively. Notice also that for $x \to 0$ and $y \to 0$ (small curvature limit), both (3.20) and (3.21) reduce to the free energy of a bimodal brush on a flat surface (3.9).

Both (3.20) and (3.21) show a minimum as a function of $1/R$, whereas the original expressions (3.15) and (3.18) decrease monotonically. For the cylindrical case, the second-order expansion (3.21) exhibits a minimum at

$$y_{\min} = \frac{3\nu}{2\nu+4}\frac{f_1(\alpha,\phi)}{f_2(\alpha,\phi)}. \tag{3.24}$$

Hence the above expansion breaks down for $h_1/2R \gtrsim y_{\min}$.

Once we have obtained the free energy of a brush bent into the inside or outside of a sphere or cylinder, we can compute the elastic moduli and the spontaneous curvature

in (1.1) using the following relations:

$$\kappa = R^2\big[F_{\rm c}(R) + F_{\rm c}(-R) - 2F_0\big], \tag{3.25}$$

$$2\kappa + \kappa_{\rm G} = \frac{1}{2}R^2\big[F_{\rm s}(R) + F_{\rm s}(-R) - 2F_0\big], \tag{3.26}$$

$$\kappa c_0 \equiv k = \frac{1}{4}R\big[F_{\rm c}(-R) - F_{\rm c}(R)\big], \tag{3.27}$$

where F_0 is the free energy of the flat brush given by (3.9). We then finally extract κ, $\kappa_{\rm G}$, and c_0 as

$$\kappa = \frac{\nu+2}{12\nu^2}TN_{\rm S}^3\Gamma^{3/2\nu}f_2(\alpha,\phi), \tag{3.28}$$

$$\kappa_{\rm G} = -\frac{1}{6\nu}TN_{\rm S}^3\Gamma^{3/2\nu}f_2(\alpha,\phi), \tag{3.29}$$

$$\kappa c_0 \equiv k = \frac{1}{8\nu}\frac{T}{a}N_{\rm S}^2\Gamma^{(2+\nu)/2\nu}f_1(\alpha,\phi), \tag{3.30}$$

where $f_1(\alpha,\phi)$ and $f_2(\alpha,\phi)$ are given by (3.22) and (3.23), respectively. These are the main new results of this paper. The calculated bending modulus is positive whereas the Gaussian modulus is negative. This means that bending into a saddle-shaped surface costs energy. For $\nu = 3/5$, the above equations become

$$\kappa = \frac{65}{108}TN_{\rm S}^3\Gamma^{5/2}f_2(\alpha,\phi), \tag{3.31}$$

$$\kappa_{\rm G} = -\frac{5}{18}TN_{\rm S}^3\Gamma^{5/2}f_2(\alpha,\phi), \tag{3.32}$$

$$k = \frac{5}{24}\frac{T}{a}N_{\rm S}^2\Gamma^{13/6}f_1(\alpha,\phi), \tag{3.33}$$

where

$$f_1(\alpha,\phi) = 1 + 2\alpha\phi^{11/6} + \alpha^2\phi^{13/6}, \tag{3.34}$$

$$f_2(\alpha,\phi) = 1 + 3\alpha\phi^{11/6} + 3\alpha^2\phi^{13/6} + \alpha^3\phi^{15/6}. \tag{3.35}$$

For either $\alpha = 0$ (monodisperse brush) or $\phi = 0$ (pure short-chain brush) which implies $f_1 = f_2 = 1$, the above results reduce to the elastic moduli and the spontaneous curvature obtained in reference [34]. We also note that for $\phi = 1$ corresponding to a pure long-chain brush, (3.22) and (3.23) become $f_1 = (1+\alpha)^2$ and $f_2 = (1+\alpha)^3$, respectively. Hence (3.28) to (3.30) become those for monodisperse brush with $N_{\rm S}$ being replaced by $N_{\rm L}$. (Notice that $N_{\rm L} = (1+\alpha)N_{\rm S}$.)

The general behavior of the functions defined $g_1 \equiv [f_1(\alpha,\phi)-1]/[f_1(\alpha,\phi=1)-1]$ and $g_2 \equiv [f_2(\alpha,\phi)-1]/[f_2(\alpha,\phi=1)-1]$ as a function of ϕ are shown in Figure 4(a) and (b), respectively, for $\nu = 3/5$ and three different values of α. Similar to Figure 2, the dependence of the elastic moduli on the volume fraction ϕ is not a simple linear interpolation between the modulus of a pure short-chain brush and a pure long-chain brush. We find that the effect of mixing a small number of long chains in a brush of mostly short chains is much less effective than the mixing of a small number of short chains in a brush of mostly long chains. This is because the long chains are strongly affected by the free volume introduced even a small number of short chains. Moreover, in the present scaling theory, the ratio $\kappa/\kappa_{\rm G}$ is a constant and given by

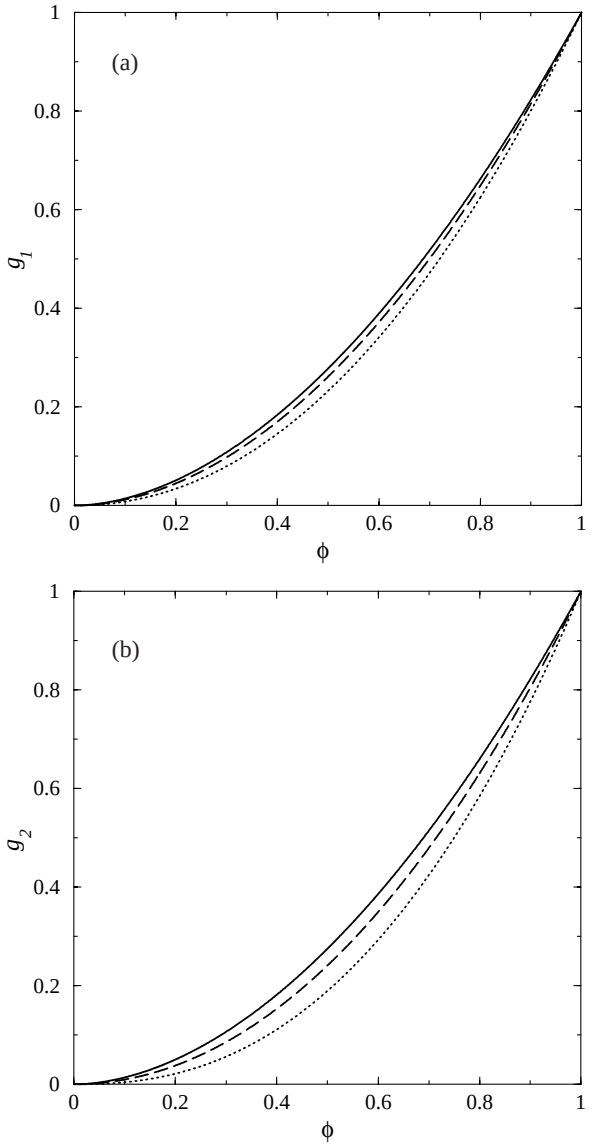

Fig. 4. Plots of (a) $g_1 \equiv [f_1(\alpha,\phi)-1]/[f_1(\alpha,\phi=1)-1]$ and (b) $g_2 \equiv [f_2(\alpha,\phi)-1]/[f_2(\alpha,\phi=1)-1]$ as a function of ϕ (fraction of longer chains) for three different values of $\alpha = 0.1$ (solid line), 1 (dashed line), and 10 (dotted line). The functions $f_1(\alpha,\phi)$ and $f_2(\alpha,\phi)$ are given by (3.34) and (3.35), respectively.

$$\frac{\kappa}{\kappa_{\rm G}} = -\frac{\nu+2}{2\nu}. \tag{3.36}$$

For $\nu = 3/5$, we have $\kappa/\kappa_{\rm G} = -13/6 \approx -2.167$.

In the case of a monodisperse brush ($f_1 = f_2 = 1$), we can compare the above expressions with those obtained by Milner and Witten for monodisperse brushes in the moderate density case using SCFT [19]. Their results are $\kappa = (9/64)(12/\pi^2)^{1/3}TN^3\Gamma^{7/3}$, $\kappa_{\rm G} = -(3/35)(12/\pi^2)^{1/3}TN^3\Gamma^{7/3}$, and $k \sim (T/a)N^2\Gamma^2$ which

are of the same sign and have the same molecular weight dependence ($\sim N^3$) as those obtained within the present scaling theory. However, the dependence on Γ is different by a factor of $\Gamma^{1/6}$. As mentioned before, this difference is due to the correlation effects which are neglected in the mean-field version of SCFT.

For a bimodal brush, the elastic moduli of a mixed brush has previously been calculated only for the *melt* case [19,30,35], and we can not directly compare this with our results. It is important to stress that α and ϕ dependence of κ and $\kappa_{\rm G}$ are exactly the same and are represented by a single function $f_2(\alpha,\phi)$ in the swollen case. This is not the case for the melt state, although it is reported that the ratio $\kappa/\kappa_{\rm G}$ is constant to within a few percent [19,30,35]. In general, the replacement of a small fraction of long-chain molecules by short-chain molecules dramatically changes the elastic moduli both for the swollen and the melt cases. Equations (3.34) and (3.35) can be expanded for $\phi \approx 1$ as

$$f_1(\alpha,\phi\to 1) \approx (1+\alpha)^2 - \frac{\alpha}{6}(22+13\alpha)(1-\phi), \quad (3.37)$$

$$f_2(\alpha,\phi\to 1) \approx (1+\alpha)^3 - \frac{\alpha}{2}(11+13\alpha+5\alpha^2)(1-\phi). \quad (3.38)$$

Hence the bending modulus and other quantities decreases linearly with $(1-\phi)$ for $\phi \approx 1$ in the present swollen case as well as in the melt case [19]. For a small fraction of long-chain molecules, the bending modulus increases as ϕ^3 in the melt case [19], whereas it increases as $\phi^{11/6}$ in the swollen case (see (3.35)) which has an even stronger effect than the melt case. (See, however, the discussion in section 5.2.)

4 Mixed amphiphilic monolayers

Up to now we have discussed the elastic properties of a bimodal brush within the scaling theory. Using the obtained results for polymer brushes, we investigate here the effect of mixing on the interfacial properties of self-assembled amphiphilic monolayers in the swollen state. Typical examples of such systems are mixtures of two AB amphiphilic diblock copolymers or surfactant molecules with different overall molecular weights and/or asymmetries, in a blend of highly incompatible solvents. For simplicity, we discuss mixed AB diblock copolymer monolayers between two immiscible solvents.

We consider the case where the solvents are inversely selective, *i.e.*, the two solvents are, respectively, good for one of the blocks and poor for the other. Then the unfavorable interaction between incompatible block-solvent pairs drives the copolymer chain to the liquid-liquid interface, and the system thereby reduces the interfacial tension. When the incompatibility between the solvents is high enough, the A-B junction points are constrained to the liquid-liquid interfaces. Since for large incompatibilities, the width of this interface is narrow compared to the chain size, one can assume that the two blocks form brush-like regions on both sides of the interface as shown in Figure 5

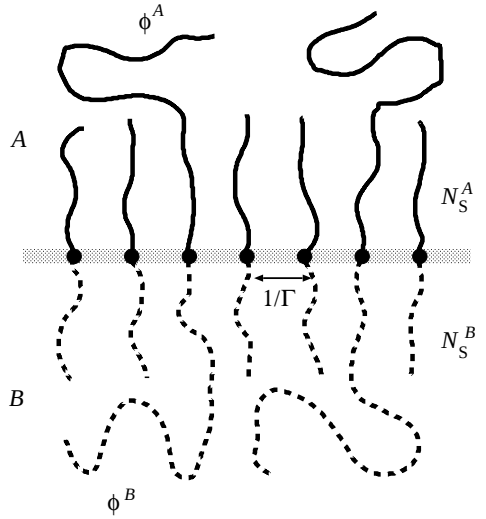

Fig. 5. Schematic diagram showing a mixed diblock copolymers at a liquid-liquid interface. When the copolymers aggregate at liquid-liquid interfaces, the A block forms a brush in one of the solvents and the B block in the other solvent. The two solvents are, respectively, good for one of the blocks and poor for the other. Hence each block is assumed to be in the swollen state. $1/\Gamma$ is the dimensionless area per chain

as long as the copolymer concentration at the interface is high enough. Hence one can calculate the elastic properties of mixed diblock interfaces by using the results for polymer brushes discussed in the previous section.

Mixed diblock monolayers in the *melt* state has been considered by Dan and Safran [30]. Here we apply their argument to the mixed monolayers in the *swollen* state. According to references [15,24,29,30], the stretching energy of a copolymer monolayer can be simply obtained by adding the stretching energies of the two block sections. For each of the blocks, the stretching energy *per unit area* is given by (1.1) which can be rewritten as

$$F_{\rm b}(c_1,c_2) = F_0 - 2k(c_1+c_2) + \frac{\kappa}{2}(c_1+c_2)^2 + \kappa_{\rm G} c_1 c_2, \quad (4.1)$$

where $F_0 = F_{\rm b}(c_1 = c_2 = 0)$ is the free energy of the brush on a flat surface given by (3.9). For our later calculations, we consider the free energy *per chain* for each of the block given by $\bar{F}_{\rm b} = F_{\rm b}/\Gamma$ and write it in the form

$$\bar{F}_{\rm b}(c_1,c_2) \equiv \Gamma^{5/6}\bar{F}_0 + \frac{1}{2}\Gamma^{7/6}\bar{k}(c_1+c_2) + \Gamma^{9/6}\left[\bar{\kappa}(c_1+c_2)^2 + \bar{\kappa}_{\rm G} c_1 c_2\right], \quad (4.2)$$

where Γ is the surface coverage given in (3.2). By using the results (3.9) and (3.28) to (3.30) in the previous section, $\bar{F}_0$, $\bar{k}$, $\bar{\kappa}$, and $\bar{\kappa}_{\rm G}$ can be defined by the unbarred quantities

by omitting the Γ dependence as

$$\bar{F}_0 \equiv \frac{T}{a^2} N_{\rm S} f_0(\alpha,\phi), \tag{4.3}$$

$$\bar{k} \equiv -\frac{5}{6}\frac{T}{a} N_{\rm S}^2 f_1(\alpha,\phi), \tag{4.4}$$

$$\bar{\kappa} \equiv \frac{65}{216} T N_{\rm S}^3 f_2(\alpha,\phi), \tag{4.5}$$

$$\bar{\kappa}_{\rm G} \equiv -\frac{5}{18} T N_{\rm S}^3 f_2(\alpha,\phi). \tag{4.6}$$

Here we have used the value $\nu = 3/5$, and $f_0(\alpha,\phi)$, $f_1(\alpha,\phi)$, and $f_2(\alpha,\phi)$ are given by (3.12), (3.34), and (3.35), respectively.

It is important to notice that, in the case of self-assembled monolayers, the surface coverage, Γ, is not fixed *a priori* as in the grafted brush, but adjusts itself to minimize the total free energy [2,15,24]. In the present case, the total free energy consists of the chain stretching contribution (4.2) and the interfacial energy. The interfacial energy is linearly proportional to the area of the liquid-liquid interfaces on which the A-B junction points are constrained. Let us take the liquid-liquid interface as the center of curvature so that the curvatures of the B block brush have signs opposite to those of the A block brush. Then the mixed free energy $\bar{F}_{\rm m}$ including both the stretching energy and the interfacial energy can be written as

$$\bar{F}_{\rm m}(\Gamma,c_1,c_2) \equiv \frac{\gamma}{\Gamma} + \bar{F}_{\rm b}^A(c_1,c_2) + \bar{F}_{\rm b}^B(-c_1,-c_2) = \frac{\gamma}{\Gamma} + \Gamma^{5/6}F + \frac{1}{2}\Gamma^{7/6}\delta(c_1+c_2) + \Gamma^{9/6}\big[(\bar{\kappa}^A+\bar{\kappa}^B)(c_1+c_2)^2 + \big(\bar{\kappa}_{\rm G}^A+\bar{\kappa}_{\rm G}^B\big)c_1c_2\big], \tag{4.7}$$

where γ is the interfacial tension,

$$F \equiv \bar{F}_0^A + \bar{F}_0^B, \tag{4.8}$$

and

$$\delta \equiv \bar{k}^A - \bar{k}^B = -\frac{5}{6}\frac{T}{a}\big[\big(N_{\rm S}^A\big)^2\big\{1+2\alpha^A\big(\phi^A\big)^{11/6}+\big(\alpha^A\big)^2\big(\phi^A\big)^{13/6}\big\} - \big(N_{\rm S}^B\big)^2\big\{1+2\alpha^B\big(\phi^B\big)^{11/6}+\big(\alpha^B\big)^2\big(\phi^B\big)^{13/6}\big\}\big]. \tag{4.9}$$

In the above, the quantities with the superscript A or B are the corresponding quantities for the A and B blocks, separately. Namely, $\bar{F}_0^J$, $\bar{k}^J$, $\bar{\kappa}^J$, and $\bar{\kappa}_{\rm G}^J$ $(J=A,B)$ are defined in (4.3) to (4.6) for $N_{\rm S}=N_{\rm S}^J$, $\alpha=\alpha^J$, and $\phi=\phi^J$, respectively. The spontaneous curvature contribution of the interface is proportional to δ. Since ϕ^J denotes the fraction of longer J blocks in the J brush, there are, in general, two possible cases [30]. The first case is a situation where the same chain contains both the longer A block and the longer B block as typically shown in Figure 6(a). In this case, $\phi^A=\phi^B$ holds. The second case is that one chain contains the longer A block, while the other chain contains the longer B block as shown in Figure 6(b). In the latter case, $\phi^A=1-\phi^B$ holds. Comparing

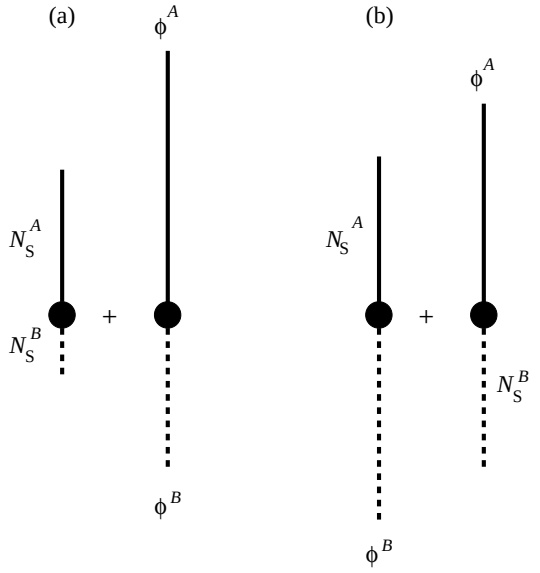

Fig. 6. Two representative mixtures of block copolymers considered in the text. (a) The two chains have the same asymmetry but different overall molecular weights, so that $\alpha^A = \alpha^B \neq 0$ and $\phi^A = \phi^B$. (b) The two chains have the same overall molecular weights, but different asymmetries, so that $N_{\rm S}^A = (\alpha^B/\alpha^A)N_{\rm S}^B$ and $\phi^A = 1-\phi^B$.

the mixed free energy for the melt case (Eq. (6) in reference [30]) with that for the swollen case (4.7), we see that (4.7) has a lower order Γ dependence. This leads to the different scaling behaviors of various interfacial properties as discussed below.

We note that ϕ^J is controlled by the experimentally imposed composition of the mixture as long as all the copolymer chains are localized at the liquid-liquid interface. However, both the surface coverage Γ and the interface curvature c_1 and c_2 are free to vary, and these quantities are determined by the minimization of the mixed free energy $\bar{F}_{\rm m}$ in (4.7). Consider a spherically deformed interface with $c_1=c_2=c$. In this case (4.7) becomes

$$\bar{F}_{\rm m}(\Gamma,c) = \frac{\gamma}{\Gamma} + \Gamma^{5/6}F + \Gamma^{7/6}\delta c + \Gamma^{9/6}Kc^2, \tag{4.10}$$

where

$$K \equiv \big(4\bar{\kappa}^A + \bar{\kappa}_{\rm G}^A\big) + \big(4\bar{\kappa}^B + \bar{\kappa}_{\rm G}^B\big), \tag{4.11}$$

which provides the overall bending modulus. As can be seen from (4.5) and (4.6), $\bar{\kappa}^A$ and $\bar{\kappa}_{\rm G}^A$ depend on $f_2(\alpha^A,\phi^A)$, while $\bar{\kappa}^B$ and $\bar{\kappa}_{\rm G}^B$ on $f_2(\alpha^B,\phi^B)$. In the case of $\alpha^A=\alpha^B$ and $\phi^A=\phi^B\equiv\phi$, for example, the ϕ dependence of the overall bending modulus K is given by Figure 4 as before, and the softening effect can be seen from (3.38).

Minimization of (4.10) with respect to both Γ and c (without any constraint) gives the equilibrium condition

$$\frac{\partial\bar{F}_{\rm m}(\Gamma,c)}{\partial\Gamma} = 0, \qquad \frac{\partial\bar{F}_{\rm m}(\Gamma,c)}{\partial c} = 0. \tag{4.12}$$

The equilibrium surface coverage is determined, to the lowest order, by the balance between the interfacial energy and the flat monolayer energy. Hence we have

$$\Gamma^{(0)} = \left(\frac{6\gamma}{5F}\right)^{6/11}, \tag{4.13}$$

which scales as $\tilde{\gamma}^{6/11}(N_{\rm S}^B)^{-6/11}$ where $\tilde{\gamma} = \gamma a^2/T$ is the dimensionless interfacial tension. The equilibrium interface curvature c is determined by the balance between the spontaneous curvature that depends linearly on $\delta = \bar{k}^A - \bar{k}^B$ (see (4.9)) and the bending modulus K (see (4.11)). To the lowest order, we have

$$c^{(0)} = -\frac{\delta}{2K}\left[\Gamma^{(0)}\right]^{-1/3} = -\frac{\delta}{2K}\left(\frac{5F}{6\gamma}\right)^{2/11}, \tag{4.14}$$

which scales as $(1/a)\tilde{\gamma}^{-2/11}(N_{\rm S}^B)^{-9/11}$. Note that the curvature vanishes for zero spontaneous curvature. Hence a flat lamellar structure is stable only when $\delta = 0$. Using the above results, the lowest-order mixing free energy turns out to be

$$F^{(0)} = \frac{11}{6}\left[\Gamma^{(0)}\right]^{5/6}F = \frac{11}{6}\left(\frac{6\gamma}{5F}\right)^{5/11}F, \tag{4.15}$$

which scales as $(T/a^2)\tilde{\gamma}^{5/11}(N_{\rm S}^B)^{6/11}$. Although the present results are for mixed monolayers, the scaling behaviors in (4.13), (4.14), and (4.15) are similar to those for monodisperse monolayers [21,36] as far as the surface tension and the chain length dependences are concerned. For mixed monolayers in the melt conditions, on the other hand, the corresponding quantities scale as $\Gamma^{(0)} \sim \tilde{\gamma}^{1/3}(N_{\rm S}^B)^{-1/3}$, $c^{(0)} \sim \tilde{\gamma}^{-1/3}(N_{\rm S}^B)^{-2/3}$ and $F^{(0)} \sim \tilde{\gamma}^{2/3}(N_{\rm S}^B)^{1/3}$ [30]. Calculating higher-order terms in a dimensionless small parameter $\delta^2/(KF)$, the equilibrium surface coverage, curvature, and mixing free energy per chain are obtained as

$$\Gamma^* = \Gamma^{(0)}\left(1 + \frac{3\delta^2}{22KF}\right), \tag{4.16}$$

$$c^* = c^{(0)}\left(1 - \frac{\delta^2}{22KF}\right), \tag{4.17}$$

$$\bar{F}_{\rm m}^* = F^{(0)}\left(1 - \frac{3\delta^2}{22KF} - \frac{15\delta^4}{1936K^2F^2}\right). \tag{4.18}$$

To see the effect of mixing on the interfacial properties of swollen monolayers, we examine here two typical mixtures of block copolymer monolayers as considered in reference [30]. Notice again that α^J and ϕ^J ($J = A, B$) are the molecular weight difference between the two chains (see (3.1)) and fraction of longer chains for each of the blocks, respectively. i) The two chains have the same asymmetry but different overall molecular weights, so that $\alpha^A = \alpha^B \neq 0$ and $\phi^A = \phi^B$ as shown in Figure 6(a). ii) The two chains have the same overall molecular weights, but different asymmetries, so that $N_{\rm S}^A = (\alpha^B/\alpha^A)N_{\rm S}^B$ and $\phi^A = 1 - \phi^B$ as shown in Figure 6(b). In the latter case one chain contains the longer A block, while the other chain contains the longer B block. In Figures 7 and 8, we have plotted Γ^*, c^*, and $\bar{F}_{\rm m}^*$ according to (4.16), (4.17), and (4.18), respectively, for these two cases. In Figure 7 (case i)), we fixed $N_{\rm S}^A = 2N_{\rm S}^B$ and considered three different values of $\alpha^A = \alpha^B = 0.1, 1, 10$; all the plots are shown as a function of $\phi \equiv \phi^A = \phi^B$. In Figure 8 (case ii)), we fixed $\alpha^A = 1$ and considered three different values of $\alpha^B = 0.1, 1, 10$; all the plots are shown as a function of $\phi \equiv \phi^A = 1 - \phi^B$.

Since the surface coverage is related to the overall interfacial area in the system (see section 5.3), Γ^* can be regarded as a measure of the emulsification efficiency of the copolymer. When $\alpha^A = \alpha^B$ is not so large ($\lesssim 1$) in case i), we find that adding a small fraction of shorter chains to a copolymer monolayer is more effective in changing the surface coverage than addition of a small fraction of longer chains (see Fig. 7(a)). This is because the stretching energy of the longer chains is considerably reduced by the presence of shorter chains which act as spacers. However, this dramatic effect of adding a small fraction of shorter chains is suppressed for larger $\alpha^A = \alpha^B = 10$. The dependence of the equilibrium surface coverage Γ^* on ϕ is non-monotonic in case ii), and each curve obtains a maximum at a finite composition (see Fig. 8(a)). The maximum point shifts to higher ϕ as α^B is increased.

The equilibrium curvature c^* is inversely proportional to the microemulsion droplet size. When $\alpha^A = \alpha^B = 0.1$ (*i.e.*, when the polymers have almost equal molecular weights) in case i), the optimal curvature c^* is almost constant for small ϕ, whereas it decreases almost linearly for ϕ close to unity (see Fig. 7(b)). However, c^* is not very much affected if a small fraction of either short or long chains are added when $\alpha^A = \alpha^B = 1$. The behavior of c^* for $\alpha^A = \alpha^B = 10$ (*i.e.*, the two polymers differ greatly in their molecular weights) is completely different. It drops sharply for small ϕ and stays almost constant for $\phi \gtrsim 0.5$. Next we discuss the ϕ dependence of c^* in case ii) in which the two chains have the same overall molecular weights but different asymmetries. From Figure 8(b), we see that for $\alpha^B = 0.1$ and 10, c^* depends only weakly on ϕ, whereas c^* changes its sign at $\phi = 0.5$ for $\alpha^B(= \alpha^A) = 1$. For the latter case, c^* just changes its sign for $\phi = 0$ and $\phi = 1$, as it should.

All the curves of the reduced free energy $\bar{F}_{\rm m}^*$ in case i) increase monotonically (see Fig. 7(c)). On the other hand, all the curves in case ii) obtain a single minimum at a finite composition (see Fig. 8(c)). In other words, there are no inflection points in both cases. Therefore the system does not tend to phase separate and the mixed monolayer is preferred. This is due to the fact that the interactions between chains of different asymmetry or molecular weights are always attractive [30]. The attractive interaction originates from the relaxation in the stretching energy by mixing shorter chains. A similar discussion has been presented by Cantor [21]. Although the scaling behaviors of various interfacial properties are different in the present swollen case and the melt case [30], the effect of mixing and the

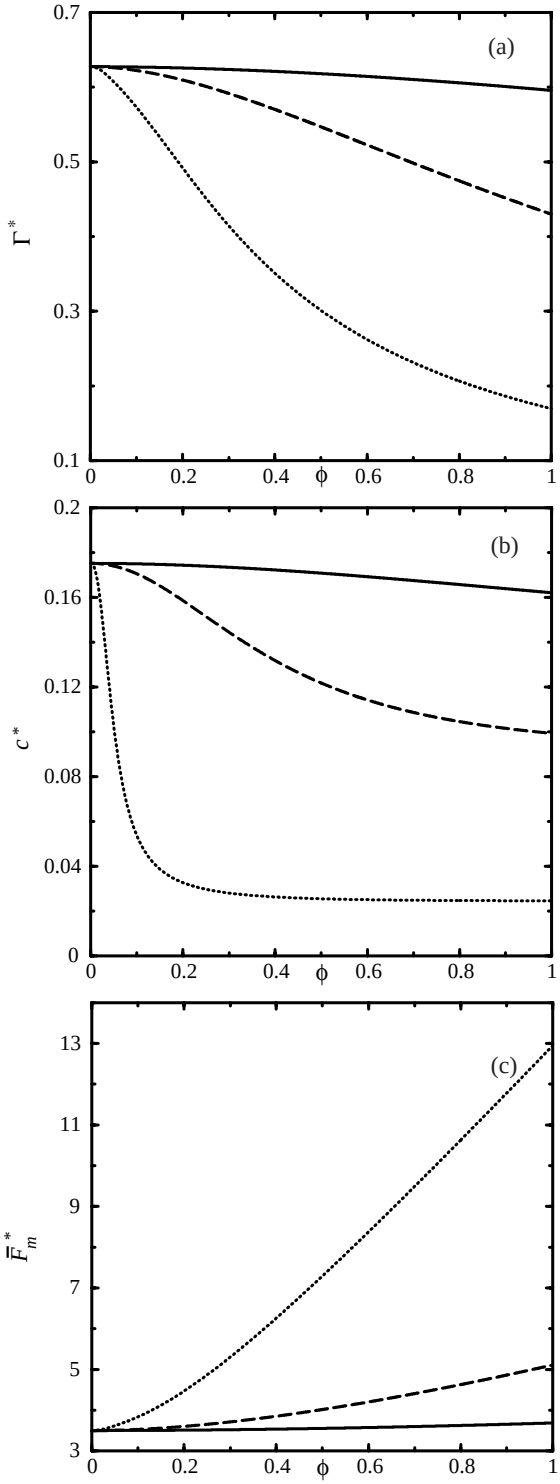

Fig. 7. Plots of equilibrium (a) surface coverage Γ^* (in units of $\gamma^{6/11}a^{12/11}T^{-6/11}(N_S^B)^{-6/11}$), (b) interface curvature c^* (in units of $\gamma^{-2/11}a^{-15/11}T^{2/11}(N_S^B)^{-9/11}$), and (c) monolayer free energy $\bar{F}_m^*$ (in units of $\gamma^{5/11}a^{-12/11}T^{6/11}(N_S^B)^{6/11}$) when the two chains have the same asymmetry but different overall molecular weights (case i) in the text or Fig. 6(a)). All the graphs are shown as a function of $\phi \equiv \phi^A = \phi^B$. The molecular weight is fixed $N_S^A = 2N_S^B$. Different curves correspond to $\alpha^A = \alpha^B = 0.1$ (solid line), 1 (dashed line), and 10 (dotted line), respectively.

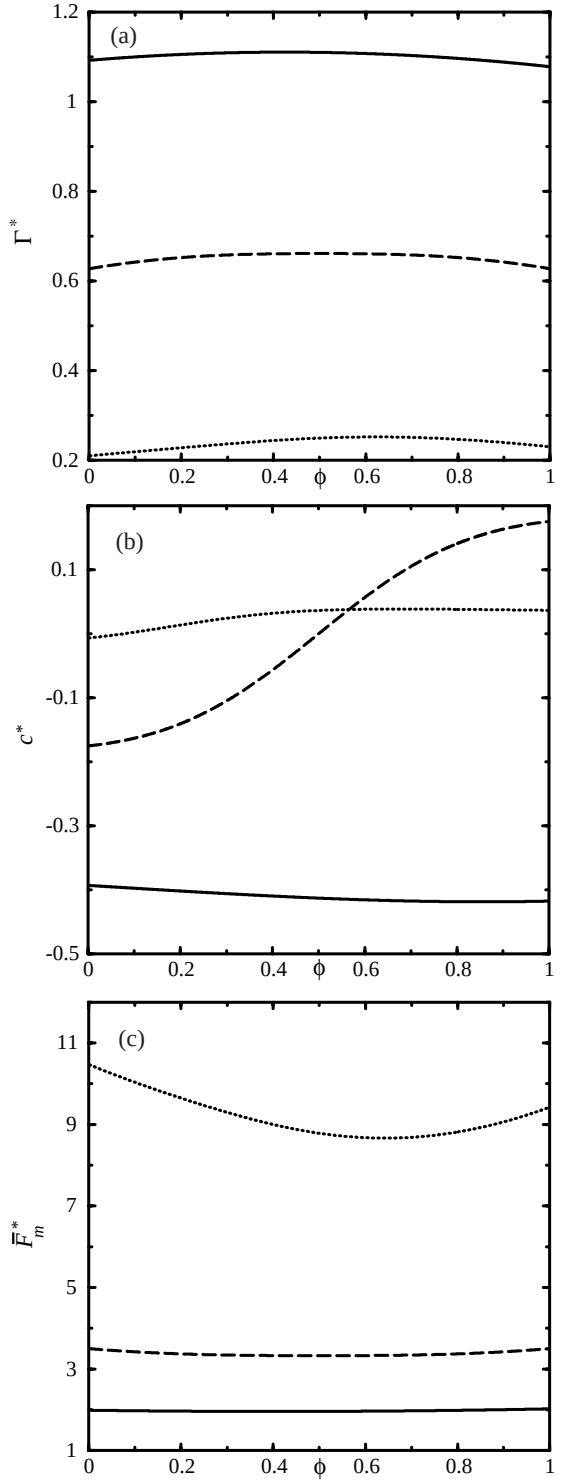

Fig. 8. Plots of equilibrium (a) surface coverage Γ^* (in units of $\gamma^{6/11}a^{12/11}T^{-6/11}(N_S^B)^{-6/11}$), (b) interface curvature c^* (in units of $\gamma^{-2/11}a^{-15/11}T^{2/11}(N_S^B)^{-9/11}$), and (c) monolayer free energy $\bar{F}_m^*$ (in units of $\gamma^{5/11}a^{-12/11}T^{6/11}(N_S^B)^{6/11}$) when the two chains have the same overall molecular weights, but different asymmetries (case ii) in the text or Fig. 6(b)). All the graphs are shown as a function of $\phi \equiv \phi^A = 1 - \phi^B$. The molecular weight is chosen as $N_S^A = (\alpha^B/\alpha^A)N_S^B$ with $\alpha^A = 1$. Different curves correspond to $\alpha^B = 0.1$ (solid line), 1 (dashed line), and 10 (dotted line), respectively.

underlying physics as discussed above, are rather similar in both cases.

Finally, we remark that the case of a cylindrical monolayer can also be calculated by putting $c_1 = c$ and $c_2 = 0$ in (4.7) and minimizing with respect to Γ and c as in the spherical case. One can obtain the equilibrium surface coverage, interface curvature, and the free energy by (4.16), (4.17), and (4.18) with δ and K being replaced by $(\bar{k}^A - \bar{k}^B)/2$ and $\bar{\kappa}^A + \bar{\kappa}^B$, respectively. However, cylindrical monolayers are unlikely to form because the free energy is always higher than that of spherical monolayers as long as there is no constraint on the volume of the microemulsion phase [30,36]. But if there are conservation constraints on the solvent, then we get the transition from spheres to cylinders or to lamellae [2].

5 Summary and discussion

5.1 Main findings

In this paper, we applied the blob model and scaling arguments of a bimodal brush, to predict the elastic and interfacial properties of mixed amphiphilic monolayers. We first extended the results in reference [34] for a flat, bimodal brush consisting of shorter and longer chains in the swollen state. Next, we calculated the elastic moduli and the spontaneous curvature as a function of the composition and the relative chain length. We obtained simple scaling functions which interpolate between the elastic moduli of a pure short-chain brush and a pure long-chain brush. We then used the analogy between block copolymer interfaces and polymeric brushes in order to calculate the stretching energy of mixed amphiphilic monolayers. Following the argument in reference [30], we discussed the effect of mixing on self-assembled diblock copolymer monolayers in the swollen state. Since the area per chain adjusts itself to minimize the total free energy in such a system, the free energy per chain is minimized with respect to both the surface coverage and the curvature. We then calculated the equilibrium surface coverage, interface curvature, and the mixing free energy as a function of the composition, and discussed their behavior for two cases of mixed, block copolymer monolayers. For a certain choice of parameters, we find that adding a small fraction of shorter chain to a copolymer monolayer is more effective in changing the surface properties than addition of a small fraction of longer chains. In general, we find a large deviation of the various surface properties from the simple linear averaging of the pure component monolayers. This nonlinear dependence on the composition is due to the effectively, attractive interactions between different types of chains, because the addition of shorter chains leads to a relaxation in the stretching energy of the longer blocks. These properties are qualitatively the same as those of mixed brushes in the melt state [30], although the scaling behavior is different between the melt and the swollen cases.

5.2 Applicability of the present theory

Although we have mainly discussed the elastic properties of mixed monolayers composed of AB diblock copolymers, one can apply our theory to mixtures of longer-chain surfactant molecules and shorter-chain surfactant molecules (cosurfactants) as considered in references [55,56]. Our result is consistent with their finding that the bending modulus is significantly reduced by the replacement of long-chain molecules by short ones. In fact, this phenomenon is experimentally observed in fluctuating flexible bilayers composed of surfactant-cosurfactant mixtures [57,58]. Strictly speaking, however, the blob picture used in this paper is valid only for long chains and the model applies to flexible diblock copolymer monolayers. Hence it should be kept in mind that the results concerning small surfactants are merely suggestive.

At the beginning of section 3, we mentioned that the brush model is inappropriate in the limit of only a few long chains. Notice that $f_1(\alpha, \phi)$ and $f_2(\alpha, \phi)$ in (3.34) and (3.35), respectively, are nonanalytic for $\phi \to 0$. This reflects the invalidity of the model in this limit. If the long chains are too dilute, the mushroom (on top of a brush) picture is relevant for the upper second layer. As described in section 2, the variation of the elastic moduli κ and $\kappa_{\rm G}$ for mushroom conformations of anchored (end-grafted) polymers has been calculated in references [33,34, 38,39]. Using their results, the elastic moduli of a bimodal brush for small ϕ can be written as

$$\kappa(\alpha, \phi \to 0) \approx \frac{65}{108} T N_{\rm S}^3 \Gamma^{5/2} + \frac{1}{12}\left(1 + \frac{\pi}{2}\right) T \frac{\alpha N_{\rm S}}{6} \Gamma\phi, \tag{5.1}$$

$$\kappa_{\rm G}(\alpha, \phi \to 0) \approx -\frac{5}{18} T N_{\rm S}^3 \Gamma^{5/2} - \frac{1}{6} T \frac{\alpha N_{\rm S}}{6} \Gamma\phi. \tag{5.2}$$

The first term in each of the equations corresponds to the elastic modulus for a pure short-chain (see (3.31) and (3.32)). The mushroom part of the long chains is assumed to be ideal and its gyration radius is given by $(\alpha N_{\rm S}/6)^{1/2}$. Note also that $\Gamma\phi$ is the effective coverage for the second upper layer, and both of the above expressions change linearly with ϕ, which is in contrast to the brush case.

5.3 Relation to experiment

Our theory may be used to interpret recent experiments on the effect of amphiphilic block copolymers on ternary microemulsions as described in the Introduction. Experimentally, the amount of surfactant molecules (C_iE_j) which is sufficient to form a one-phase microemulsion can be dramatically reduced by the addition of a small amount of amphiphilic block copolymers (PEP-PEO) [31,32]. The neutron scattering experiments showed that the above finding is connected to the increase in the structural length scale d (typical size of an oil or water domain) of the microemulsion [31]. For small concentrations of copolymers,

mushroom picture predicts that the observed solubility enhancement is attributed to the variation of the elastic moduli [32]. For relatively high copolymer concentrations, however, the brush regime is entered and the mushroom picture ceases to be valid. In this case our theory can be applied. The surfactant molecules and amphiphilic block copolymers in the experiment correspond to shorter and longer chains in our theory, respectively.

We now briefly explain why the change in the bending modulus affects the structural length scale of the microemulsion [2]. We denote the number of surfactant molecules *per unit volume* by n. Then the domain size d is roughly related to n by [59]

$$d \sim \frac{\Gamma}{na^2}. \tag{5.3}$$

This domain size should be compared with the persistence length $\ell_{\rm p}$ of the monolayer defined by [59,60]

$$\ell_{\rm p} \sim a \exp\left(\frac{\kappa}{T}\right). \tag{5.4}$$

The interface remains flat over distances smaller than $\ell_{\rm p}$ but is crumpled at larger length scales. For $\ell_{\rm p} > d$, the monolayers tend to be parallel to each other, whereas for $\ell_{\rm p} < d$, the monolayers are wrinkled and can form microemulsions [59,61–64]. Therefore, as a rough estimate of the minimum surfactant concentration $n_{\rm c}$ needed to solubilize oil and water, we set $\ell_{\rm p} \sim d$ and obtain

$$n_{\rm c} \sim \frac{\Gamma}{a^3} \exp\left(-\frac{\kappa}{T}\right). \tag{5.5}$$

Since $n_{\rm c}$ decreases exponentially with κ, the efficiency boost can reflect an increase in κ [31,32]. It may be then convenient to define an emulsification enhancement factor η given by $\eta \equiv \exp(\Delta\kappa/T)$, where $\Delta\kappa$ is the change of the bending modulus due to the presence of the added longer chains.

When the volume fraction of the block copolymer is sufficiently small, each copolymer may be considered to be in the mushroom regime. The change of the bending modulus in the mushroom regime has been calculated by several authors in references [33,34,38,39]. In that case, the enhancement factor can be given (ignoring some numerical factors)

$$\eta_{\rm mush} \sim \exp\left(N_{\rm L}\Gamma\right), \tag{5.6}$$

for $N_{\rm L} \gg N_{\rm S}$. However, it is important to notice that the polymer mushroom influences the properties of the interface only on a scale of the order of polymer size. The uniform distribution of the curvature is correct only when mushrooms just begin to overlap [32]. When the volume fraction of the copolymer is high enough to form brushes, one should use the expression of the bending modulus calculated in this paper or in reference [34]. Using (3.28), the enhancement factor is given by

$$\eta_{\rm brush} \sim \exp\left(N_{\rm L}^3\Gamma^{5/2}\right) \sim \exp\left(N_{\rm L}^{18/11}\right), \tag{5.7}$$

for $N_{\rm L} \gg N_{\rm S}$ and we have used (4.13). Notice that $\eta_{\rm brush}$ has a much stronger dependence on $N_{\rm L}$ and Γ than in $\eta_{\rm mush}$. Hence the solubility enhancement should be much more dramatic in the brush regime. When $N_{\rm L} = 100$, for example, the overlap coverage is $\Gamma_{\rm ov} \approx 0.004$. At this surface coverage, the enhancement factor in the mushroom and brush regimes are $\eta_{\rm mush} \approx 1.49$ and $\eta_{\rm brush} \approx 2.75$, respectively. A combination of these two regimes would account for the effect of the added block copolymers on the microemulsions in both the mushroom and brush regimes.

We have greatly benefited from the discussions and correspondence with N. Dan and R. Strey. SK thanks the Ministry of Education, Science and Culture, Japan for providing financial support during his visit to Weizmann Institute of Science, Israel. Support from the exchange program between the Japan Society for the Promotion of Science (JSPS) and the Israel Ministry of Science and Technology is also gratefully acknowledged. SAS is grateful to the Israel Science Foundation for its sponsorship of the Center on Self Assembly and to the donors of the Petroleum Research Fund administered by the American Chemical Society.

Appendix A. Bimodal brush on a sphere and a cylinder

In this appendix we derive the free energy of a bimodal brush on a sphere and a cylinder. First we consider the spherical surface as illustrated in Figure 3. The brush height of the first layer $h_{1\rm s}(R)$ is implicitly given by the following equation:

$$N_{\rm S} = \int_R^{R+h_{1\rm s}} {\rm d}r \left(\frac{\xi_{1\rm s}(r)}{a}\right)^{1/\nu} \left(\frac{1}{\xi_{1\rm s}(r)}\right). \tag{A.1}$$

From (3.14), this leads to

$$h_1 = \nu R\left[\left(1+\frac{h_{1\rm s}(R)}{R}\right)^{1/\nu} - 1\right], \tag{A.2}$$

where h_1 is the height of the first layer in the flat case and is given by (3.4). Solving this equation for $h_{1\rm s}(R)$, we obtain

$$h_{1\rm s}(R) = R\left[\left(1+\frac{h_1}{\nu R}\right)^{\nu} - 1\right]. \tag{A.3}$$

This equation is the same as equation (48) in reference [34] which treats the *monodisperse* case. For the second layer, the height of the brush $h_{2\rm s}(R)$ satisfies the equation

$$N_{\rm L} - N_{\rm S} = \int_{R+h_{1\rm s}}^{R+h_{1\rm s}+h_{2\rm s}} {\rm d}r \left(\frac{\xi_{2\rm s}(r)}{a}\right)^{1/\nu} \left(\frac{1}{\xi_{2\rm s}(r)}\right). \tag{A.4}$$

From (3.14), this leads to

$$h_2 = \nu R\left[\left\{\frac{h_{2\rm s}(R)}{R} + \left(1+\frac{h_1}{\nu R}\right)^{\nu}\right\}^{1/\nu} - \left(1+\frac{h_1}{\nu R}\right)\right], \tag{A.5}$$

where h_2 is the height of the second layer in the flat case and is given by (3.6). Solving this equation for $h_{2s}(R)$, we obtain

$$h_{2s}(R) = R\left[\left(1+\frac{h_1+h_2}{\nu R}\right)^{\nu} - \left(1+\frac{h_1}{\nu R}\right)^{\nu}\right]. \quad \text{(A.6)}$$

Similar to the flat surface, the total free energy $\tilde{F}_s$ of a bimodal brush on a spherical surface is proportional to the number of blobs. Thus it can be calculated (to within a constant of order unity) as

$$\tilde{F}_s = T\left[\left(\frac{A}{\xi_0^2}\right)\int_R^{R+h_{1s}} \mathrm{d}r \frac{1}{\xi_{1s}(r)} + \left(\frac{A}{\xi_0^2/\phi}\right)\int_{R+h_{1s}}^{R+h_{1s}+h_{2s}} \mathrm{d}r \frac{1}{\xi_{2s}(r)}\right], \quad \text{(A.7)}$$

where $\xi_{1s}(r)$ and $\xi_{2s}(r)$ are given by (3.14), h_{1s} and h_{2s} are given by (A.3) and (A.6), respectively. After some calculations, the free energy *per unit area* defined by $F_s = \tilde{F}_s/A$ is given by (3.15).

Next we consider the cylindrical surface case. The brush height of the first layer $h_{1c}(R)$ implicitly satisfies an equation analogous to (A.1) with h_{1s} and $\xi_{1s}(r)$ being replaced by h_{1c} and $\xi_{1c}(r)$, respectively. Using (3.17) and solving for $h_{1c}(R)$, we have

$$h_{1c}(R) = R\left[\left(1+\frac{(1+\nu)h_1}{2\nu R}\right)^{2\nu/(1+\nu)} - 1\right]. \quad \text{(A.8)}$$

This equation is the same as equation (51) in reference [34] which treated the *monodisperse* case. Similarly, the height of the second layer $h_{2c}(R)$ satisfies an equation analogous to (A.4). We then solve for $h_{2c}(R)$ to obtain

$$h_{2c}(R) = R\left[\left(1+\frac{(1+\nu)(h_1+h_2)}{2\nu R}\right)^{2\nu/(1+\nu)} - \left(1+\frac{(1+\nu)h_1}{2\nu R}\right)^{2\nu/(1+\nu)}\right]. \quad \text{(A.9)}$$

We calculate the the total free energy $\tilde{F}_c$ analogous to (A.7), and convert to the free energy *per unit area* $F_c = \tilde{F}_c/A$. Then we obtain (3.18).

References

1. W. Helfrich, Z. Naturforsch. **28c**, 693 (1973).
2. S.A. Safran, *Statistical Thermodynamics of Surface, Interfaces, and Membranes* (Addison-Wesley, New York, 1994).
3. G. Gompper, M. Schick, *Self-Assembling Amphiphilic Systems* (Academic Press, London, 1994).
4. W.M. Gelbart, A. Ben-Shaul, D. Roux, (Editors), *Micelles, Membranes, Microemulsions, and Monolayers* (Springer-Verlag, New York, 1994).
5. S.A. Safran, Adv. in Physics **48**, 395 (1999).
6. A. Halperin, M. Tirrel, T.P. Lodge, Adv. Polym. Sci. **100**, 31 (1991).
7. I.W. Hamley, *The Physics of Block Copolymers* (Oxford University Press, New York, 1998).
8. F.S. Bates, W.W. Maurer, P.M. Lipic, M.A. Hillmyer, K. Almdal, K. Mortensen, G.H. Fredrickson, T.P. Lodge, Phys. Rev. Lett. **79**, 849 (1997).
9. G.H. Fredrickson, F.S. Bates, J. Polym. Sci.: Part B: Polym. Phys. **35**, 2775 (1997).
10. M.A. Hillmyer, W.W. Maurer, T.P. Lodge, F.S. Bates, J. Phys. Chem. B **103**, 4814 (1999).
11. T.L. Morkved, B.R. Chapman, F.S. Bates, T.P. Lodge, P. Stepanek, K. Almdal, Faraday Discuss. **112**, 335 (1999).
12. P.G. de Gennes, J. Phys. (Paris) **37**, 1445 (1976).
13. P.G. de Gennes, Macromolecules **13**, 1069 (1980).
14. S. Alexander, J. Phys. (Paris) **38**, 983 (1977).
15. Z.-G. Wang, S.A. Safran, J. Phys. (Paris) **51**, 185 (1990).
16. S.T. Milner, T.A. Witten, M.E. Cates, Europhys. Lett. **5**, 413 (1988).
17. S.T. Milner, T.A. Witten, M.E. Cates, Macromolecules **21**, 2610 (1988).
18. S.T. Milner, T.A. Witten, M.E. Cates, Macromolecules **22**, 853 (1989).
19. S.T. Milner, T.A. Witten, J. Phys. (Paris) **49**, 1951 (1988).
20. T.M. Birshtein, Y.V. Liatskaya, E.B. Zhulina, Polymer **31**, 2185 (1990).
21. R. Cantor, Macromolecules **14**, 1186 (1981).
22. L. Leibler, Makromol. Chem. Macromol. Symp. **16**, 1 (1989).
23. L. Leibler, Physica A **172**, 258 (1991).
24. Z.-G. Wang, S.A. Safran, J. Chem. Phys. **94**, 679 (1991).
25. E.W. Kaler, A.K. Murthy, B.E. Rodriguez, J.A.K. Zasadzinski, Science **245**, 1371 (1989).
26. S.A. Safran, P.A. Pincus, D. Andelman, Science **248**, 354 (1990).
27. S.A. Safran, P.A. Pincus, D. Andelman, F.C. MacKintosh, Phys. Rev. A **43**, 1071 (1991).
28. F.C. MacKintosh, S.A. Safran, Phys. Rev. E **47**, 1180 (1993).
29. N. Dan, S.A. Safran, Europhys. Lett. **21**, 975 (1993).
30. N. Dan, S.A. Safran, Macromolecules **27**, 5766 (1994).
31. B. Jakobs, T. Sottmann, R. Strey, J. Allgaier, L. Willner, D. Richter, Langmuir **15**, 6707 (1999).
32. H. Endo, J. Allgaier, G. Gompper, B. Jakobs, M. Monkenbusch, D. Richter, T. Sottmann, R. Strey, Phys. Rev. Lett. **85**, 102 (2000).
33. R. Lipowsky, Europhys. Lett. **30**, 197 (1995).
34. C. Hiergeist, R. Lipowsky, J. Phys. II **6**, 1465 (1996).
35. In reference [30] the authors point out that there are misprints in equations (32) and (37) of reference [19] for the bending and Gaussian moduli of a bimodal brush in the melt case, and claim that equations (3) to (5) in reference [30] are the correct forms. However, we still find some misprints there. For example, $\kappa(\phi,\alpha)$ in equation (4) of reference [30] does not give a correct limit for $\phi \to 1$. Moreover $\kappa(\phi,\alpha)$ *decreases* for small ϕ for fixed α, which is unphysical. Also $\bar{\kappa}(\phi,\alpha)$ in equation (5) should be proportional to N_s^3.
36. N. Dan, M. Tirrell, Macromolecules **26**, 637 (1993).
37. A.N. Semenov, Sov. Phys. JETP **61**, 733 (1985).
38. E. Eisenriegler, A. Hanke, S. Dietrich, Phys. Rev. E **54**, 1134 (1996).
39. C.M. Marques, J.B. Fournier, Europhys. Lett. **35**, 361 (1996).
40. H. Ji, D. Hone, Macromolecules **21**, 2600 (1988).

41. P.G. de Gennes, J. Phys. Chem. **94**, 8407 (1990).
42. J.T. Brooks, C.M. Marques, M.E. Cates, Europhys. Lett. **14**, 713 (1991).
43. J.T. Brooks, C.M. Marques, M.E. Cates, J. Phys. II **1**, 673 (1991).
44. K. Hristova, D. Needham, J. Colloid Int. Sci. **168**, 302 (1994).
45. K. Hristova, D. Needham, Macromolecules **28**, 991 (1995).
46. H.E. Warriner, S.H.J. Idziak, N.L. Slack, P. Davidson, C.R. Safinya, Science **271**, 9699 (1996).
47. S.L. Keller, H.E. Warriner, C.R. Safinya, J.A. Zasadzinski, Phys. Rev. Lett. **78**, 4781 (1997).
48. H.E. Warriner, P. Davidson, N.L. Slack, M. Schellhorn, P. Eiselt, S.H.J. Idziak, H.-W. Schmidt, C.R. Safinya, J. Chem. Phys. **107**, 9 (1997).
49. R. Joannic, L. Auvray, D.D. Lasic, Phys. Rev. Lett. **78**, 3402 (1997).
50. E. Evans, W. Rawicz, Phys. Rev. Lett. **79**, 2379 (1997).
51. Y. Yang, R. Prudhomme, K. M. McGrath, P. Richetti, C.M. Marques, Phys. Rev. Lett. **80**, 2729 (1998).
52. F. Castro-Roman, G. Porte, C. Ligoure, Phys. Rev. Lett. **82**, 109 (1999).
53. P.G. de Gennes, *Scaling Concepts in Polymer Physics* (Cornell University Press, New York, 1979).
54. In order to compare with the expressions in references [14, 34], one has to consider the free energy *per chain* and hence divide (3.11) by Γ.
55. I. Szleifer, D. Kramer, A. Ben-Shaul, D. Roux, W. M. Gelbart, Phys. Rev. Lett. **60**, 1966 (1988).
56. I. Szleifer, D. Kramer, A. Ben-Shaul, W. M. Gelbart, S.A. Safran, J. Chem. Phys. **92**, 6800 (1990).
57. M. DiMeglio, M. Dvolaitzky, C. Taupin, J. Phys. Chem. **89**, 871 (1985).
58. C.R. Safinya, E.B. Sirota, D. Roux, G.S. Smith, Phys. Rev. Lett. **62**, 1134 (1989).
59. P.G. de Gennes, C. Taupin, J. Phys. Chem. **86**, 2294 (1982).
60. In the exponential, we have ignored a numerical factor which is the order of unity, and used the segment size a as a lower cut-off in the wavelength of the undulations.
61. D. Andelman, M.E. Cates, D. Roux, S.A. Safran, J. Chem. Phys. **87**, 7229 (1987).
62. L. Golubović, Phys. Rev. E **50**, R2419 (1994).
63. D.C. Morse, Phys. Rev. E **50**, R2423 (1994).
64. G. Gompper, D.M. Kroll, Phys. Rev. Lett. **81**, 2284 (1998).